Magnetoplasmon excitations in quasi-two-dimensional Rashba spintronic systems: Oscillations, resonances, and energy gaps

Manvir S. Kushwaha
Institute of Physics, University of Puebla, P.O. Box J-45, Puebla 72570, Mexico
(Received 22 March 2006; published 11 July 2006)

We report on the theoretical investigation of plasmon excitations in a quasi-two-dimensional electron gas (2DEG) in the presence of a perpendicular magnetic field and spin-orbit interaction induced by the Rashba effect. We derive and discuss the dispersion relations for charge-density excitations within the framework of Bohm-Pines' random-phase approximation. The magnetoplasmons in a 2DEG are known to be characterized by two important properties: (i) the oscillatory behavior of the dispersion curves in the short wavelength limit (SWL) and (ii) the resonance splitting at the frequency $\omega=n\omega_c$ in the long wavelength limit (LWL); n ($\geqslant 2$) being an integer and ω_c the cyclotron frequency. Here we study the effect of the Rashba spin-orbit interactions (SOIs) on these characteristics in depth. We observe that the SOI modifies drastically both the oscillatory behavior in the SWL and yields multiple resonance splittings [at $\omega=(n\pm x_0)\omega_c$] in the LWL. Such resonance splittings make the spintronic systems potential candidates for quantum-well-based new devices as spin filters. We discuss the dependence of the magnetoplasmon energy on the propagation vector, the magnetic field, the 2D charge-density, and the Rashba parameter characterizing the SOI.

DOI: 10.1103/PhysRevB.74.045304 PACS number(s): 71.70.Ej, 72.25.Dc, 73.21.Fg, 73.43.Lp

I. INTRODUCTION

Semiconducting systems guarantee the zero-field spin degeneracy only in the presence of spatial inversion symmetry. Any inversion asymmetry in the system can lead to the spin splitting even in the absence of an external magnetic field. Two basic mechanisms that cause a zero-field spin-splitting are directly related to the symmetry properties of the semiconducting heterostructures. They stem from the bulk inversion asymmetry (BIA) predicted by Dresselhaus[1] and the structure inversion asymmetry (SIA) proposed by Rashba.[2] It has become known that the Dresselhaus (Rashba) mechanism dominates in the wide-gap (narrow-gap) semiconducting systems. In the intermediate-gap systems, such as GaAs quantum wells, both mechanisms are of comparable magnitude.[3]

Recent years have seen a great deal of research interest in the spin dynamics associated with the emerging field of spintronics.[4] Spintronics is based in part on manipulation of the spin degree of freedom of the carriers to develop novel features and functionalities for solid state devices. Basic design proposals for spintronic devices with wide range of applications, such as spin transistors,[5] quantum computing,[6] field-effect switches,[7] spin filters,[8] data storage,[9] etc., rely on the fact that electron waves with opposite spin acquire a phase difference during their propagation in the presence of the Rashba effect. This is a gate voltage induced spin-splitting of band edge states in the absence of an applied magnetic field.

The dramatic progress made on the miniaturization (of size and dimensions) leading to such manmade systems as quantum wells, wires, dots, and modulated systems,[10] has in recent years evolved into the study of the narrow-gap semiconductors, most notably InAs, and the important role they play in the rapidly evolving field of spintronics. As a nonmagnetic element in hybrid devices, these semiconductor materials are expected to help control the electron spin states just as the electron charge is controlled in the conventional electronic devices. One key idea of such devices is that the spin-orbit interaction (SOI) in narrow-gap semiconductors causes the spins of the carriers to precess. This was conceived by Datta and Das in a seminal paper,[5] which describes how the external gate electrode can be used to manipulate the SOI provided that the latter depends on the interface electric field, the so-called Rashba effect. The experimental results[4] reveal that, in InAs- and InGaAs-based two-dimensional electron gas (2DEG) systems, the zero-field spin-splitting[11,12] is mainly caused by Rashba effect, which can be enhanced further by increasing the gate voltage applied.

In the present paper, we investigate the electron spin dynamics in $In_{1-x}Ga_xAs/In_{1-x}Al_xAs$ quantum wells within the lowest occupied (electric) subband in the presence of an applied perpendicular magnetic field in the framework of Bohm-Pines' random-phase approximation (RPA).[13] The role of an applied magnetic field to probe the treasure of conventional solids has been appreciated long before the advent of the nonconventional solids.[14] This is because the effect of the magnetic field on the band structure is more striking and is easily observed in the experiments. A number of interesting phenomena originate from the alteration in the band structure due to the magnetic field, such as the Bloch states yielding metallic conductivity,[15] the Landau diamagnetism,[16] the Subhnikov–de Haas effect,[17] the de Haas–van Alphen effect,[18] cyclotron resonance,[19] appealing Hofstadter butterfly spectrum,[20] 2D extended states below the localized Fermi energy responsible for the quantum Hall effect,[21] to name a few. These have been investigated and serve as the diagnostic tools for characterizing the materials. As to the excitement in the spintronics, the recent discovery of spin-Hall effect in 2DEG,[22–25] within different physical contexts, is known to have added new dimensions to the spintronic research.

A two-dimensional electron gas in the presence of an applied perpendicular magnetic field is well known for mani-

festing numerous interesting basic properties. These are, for instance, the quantization of Landau levels and the resulting gaps in the density of states, and the Fermi energy oscillating as a function of the magnetic field. The latter entails the oscillations in the total energy, the magnetization, the thermoelectric power, and the specific heat as a function of an applied magnetic field.[10] As regards the orientation of the magnetic field, there are, in principle, several possible geometries, such as Faraday, Voigt, perpendicular, and (in general) tilted configurations.[10] But the perpendicular geometry, when the quantizing magnetic field is parallel to the confining electric field, is very special, particularly in the 2D electron systems. This is because only in the perpendicular geometry does the system attain the state of *complete* quantization and thus provides an ideal tool for studying quantum transport phenomena.

Our aim here is specifically to explore systematically the role of Rashba SOI on the magnetoplasmons in a 2DEG. The magnetoplasmons in a 2DEG (without SOI) are since long known[10,26] to possess the following interesting properties: (i) the oscillatory behavior of the dispersion curves in the short wavelength limit (SWL) and (ii) the resonance splitting at the frequency $\omega=n\omega_c$ in the long wavelength limit (LWL). Here n ($\geqslant 2$) is an integer and $\omega_c=eB/m^*c$ the cyclotron frequency, with e as the electronic charge, B the intensity of the magnetic field, m^* the effective mass of the charge carriers, and c the speed of light in vacuum. The presence of the Rashba SOI is observed to modify the magnetoplasmon dispersion in the following ways: (i) the nearest resonances are seen to appear at $\omega=(n\pm x_0)\omega_c$, where x is a noninteger, (ii) the major next-nearest resonances are seen to occur at $\omega=(n+y_0)\omega_c$, where $y_0(\neq x_0)\gtrless 0$, (iii) the energy gaps increase with increasing magnetic field, (iv) the energy gaps decrease with increasing 2D charge density, (v) the resonant modes move farther apart with increasing α (the Rashba parameter that defines the SOI strength) and the energy gaps feel significant variations in their magnitude, (vi) for a given propagation vector, the magnetoplasmon dispersion is sensitive and significant only at the higher (lower) values of $\alpha(B)$, etc.

The rest of the paper is organized as follows. Section II is the principal part of the paper which is devoted to the solution of the problem and to the analysis of the results obtained within the RPA. There we present our mathematical formalism for the quasi-two-dimensional electron gas (Q2DEG) in the presence of an applied magnetic field and the SOI due to Rashba mechanism and derive the required nonlocal, dynamic dielectric function. Section III is devoted to discuss several illustrative examples on the magnetoplasmon excitations for various case studies. We conclude our finding with specific remarks in Sec. IV.

II. MATHEMATICAL FORMALISM

For a typical 2DEG in the x-y plane with a magnetic field applied along the z direction in the Landau gauge [$\mathbf{A}=(-By,0,0)$] in narrow-gap semiconductors, such as $In_{1-x}Ga_xAs/In_{1-x}Al_xAs$ quantum wells, the single-particle (of charge $-e$, with $e>0$) Hamiltonian including the lowest order of the spin-orbit interactions can be expressed as

$$H=\frac{1}{2m^*}\left(\hat{\mathbf{p}}+\frac{e}{c}\hat{\mathbf{A}}\right)^2+\frac{\alpha}{\hbar}\left[\hat{\sigma}\times\left(\hat{\mathbf{p}}+\frac{e}{c}\hat{\mathbf{A}}\right)\right]_z+\frac{1}{2}g^*\mu_B B\sigma_z+V_c(z), \tag{1}$$

where α is the Rashba parameter, which describes the strength of the SOI, $\hat{\sigma}\equiv(\sigma_x,\sigma_y,\sigma_z)$ stands for vector of the Pauli spin matrices, $\hat{\mathbf{p}}$ is the momentum operator, g^* is the electron g factor, $\mu_B=e\hbar/(2m_0c)$ is the Bohr magneton, and the rest of the symbols have their usual meanings. We assume the electrons to be confined in the x-y plane due to a relatively stronger confinement potential $V_c(z)$. The first, second, and third terms in Eq. (1) represent, respectively, the orbital, Rashba, and Zeeman Hamiltonians. Such a system is characterized by the eigenfunctions

$$\psi_{nl}^{+}(k_x)=\frac{1}{\sqrt{L_xA_l}}e^{ik_xx}\begin{pmatrix}\beta\phi_{l-1}(y-y_c)\\ \phi_l(y-yc)\end{pmatrix}\phi_n(z) \tag{2}$$

and

$$\psi_{nl}^{-}(k_x)=\frac{1}{\sqrt{L_xA_l}}e^{ik_xx}\begin{pmatrix}\phi_{l-1}(y-y_c)\\ \beta\phi_l(y-yc)\end{pmatrix}\phi_n(z) \tag{3}$$

and the eigenenergies

$$\epsilon_{nl}^{\pm}=l\hbar\omega_c\pm\left[\epsilon_0^2+2l\left(\frac{\alpha}{l_c}\right)^2\right]^{1/2}+\epsilon_n. \tag{4}$$

In Eqs. (2) and (3), the function $\phi_l(x)$, with $x=(y-y_c)$, is the Hermite function defined as

$$\phi_l(x)=N_le^{-x^2/2l_c^2}H_l(x/l_c), \tag{5}$$

where $N_l=1/\sqrt{\sqrt{\pi}2^l l!l_c}$ is the standard normalization constant. Other symbols used in Eqs. (2)–(5) are defined as follows:

$$\beta=-iD_l,$$

$$A_l=1+D_l^2,$$

$$D_l=\frac{\sqrt{2l}(\alpha/l_c)}{\epsilon_0+\sqrt{\epsilon_0^2+2l(\alpha/l_c)^2}},$$

$$\epsilon_0=\frac{1}{2}(\hbar\omega_c-g\mu_BB),$$

$$l_c=\sqrt{\hbar/m^*\omega_c},$$

$$\omega_c=\frac{eB}{m^*c},$$

$$y_c=k_xl_c^2. \tag{6}$$

Here L_x, l, l_c, ω_c, and y_c are, respectively, the normalization length, the Landau level index, the magnetic length, the cyclotron frequency, and the center of the cyclotron orbit. In Eq. (4), ϵ_n is the energy of the nth (electric) subband and

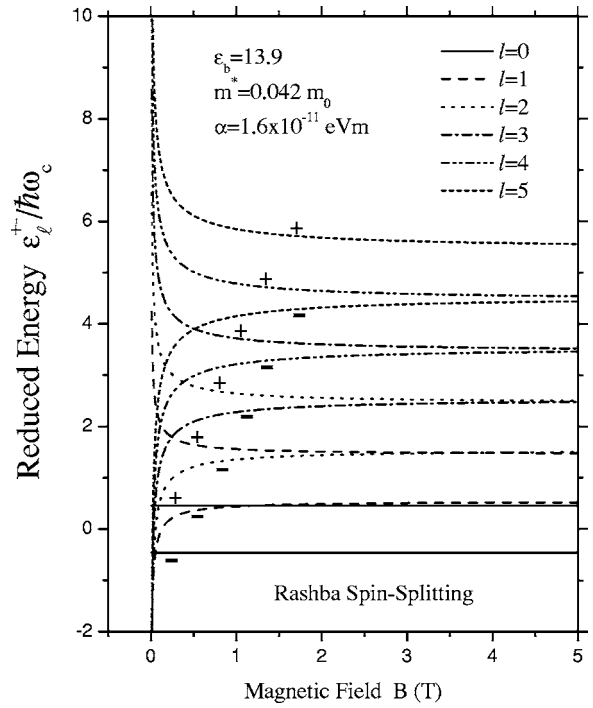

FIG. 1. The dimensionless eigenenergies $\epsilon_l^{\pm}/\hbar\omega_c$ as a function of magnetic field B, for a given value of $\alpha=1.6\times10^{-11}$ and Landau level l. Notice the spin-up (+) and the spin-down (−) energy variation for a given value of Landau level l. The solid lines stand for $l=0$.

$\phi_n(z)$ the corresponding wave function due to the confinement along the z direction.

Let us focus on the eigenenergies given by Eq. (4). In Fig. 1, we have plotted the dimensionless energy $\epsilon_l^{\pm}/\hbar\omega_c$ as a function of magnetic field B, for a given value of α. The important characteristic of this dispersion relation is that the spin splitting is larger at the lower values of B; specifically, the spin-up (spin-down) eigenenergy decreases (increases) nonlinearly with increasing values of B, for a given Landau level l. At the higher values of the magnetic field ($B\gtrsim3$ T), both spin-up and spin-down energies tend to become nondispersive and the spin-splitting is virtually defined by an effective Zeeman energy $[\Delta\approx(l\hbar\omega_c\pm\epsilon_0)]$. This is because at the higher values of B, the second term inside the square bracket starts diminishing and finally becomes negligible as compared to the first. This description is valid for nonzero values of l. For $l=0$, the spin-splitting is always constant (i.e., nondispersive) and is simply given by $\pm\epsilon_0$. This is clearly demonstrated in Fig. 1.

In the absence of any SOI and the Zeeman energy, the eigenfunction and the eigenenergy take the following well-known forms:

$$\psi_{nl}(k_x)=\frac{1}{\sqrt{L_x}}e^{k_x x}\phi_l(y-y_c)\phi_n(z) \tag{7}$$

and

$$\epsilon_{nl}=\left(l+\frac{1}{2}\right)\hbar\omega_c+\epsilon_n. \tag{8}$$

We start with a general expression for the single-particle density-density response function (DDRF) $\chi^0(\cdots)$ given by[10]

$$\chi^0(\mathbf{r},\mathbf{r}';\omega)=\sum_{\zeta\zeta'}\Lambda_{\zeta\zeta'}\psi_\zeta^*(\mathbf{r}')\psi_{\zeta'}(\mathbf{r}')\psi_{\zeta'}^*(\mathbf{r})\psi_\zeta(\mathbf{r}), \tag{9}$$

where $\mathbf{r}\equiv(x,y,z)$, $\zeta\equiv\{i,\sigma\}$, with $i\equiv\{k_x,n,l\}$ and $\sigma\equiv\pm1$, and the (general) polarizability function $\Lambda_{\zeta\zeta'}$ is defined as

$$\Lambda_{\zeta,\zeta'}\equiv\Lambda_{ij}^{\sigma\sigma'}\equiv\Lambda_{\substack{nn'\\ll'}}^{\sigma\sigma'}=\frac{f(\epsilon_{nl}^{\sigma})-f(\epsilon_{n'l'}^{\sigma'})}{\epsilon_{nl}^{\sigma}-\epsilon_{n'l'}^{\sigma'}+\hbar\omega^*}, \tag{10}$$

where $f(x)$ is the well-known Fermi distribution function. $\omega^*=w+i\gamma$ and small but nonzero γ represents the adiabatic switching of the Coulomb interactions in the remote past. For the sake of simplicity, we rewrite Eqs. (2) and (3) symbolically as follows:

$$\psi_\zeta(\mathbf{r})=\phi_{k_x}(x)\phi_{\sigma l}(y-y_c)\phi_n(z), \tag{11}$$

where

$$\phi_{k_x}(x)=\frac{1}{\sqrt{L_xA_l}}e^{ik_xx} \tag{12}$$

and

$$\phi_{\sigma l}(y-y_c)=\begin{cases}\begin{pmatrix}\beta\phi_{l-1}(y-y_c)\\ \phi_l(y-yc)\end{pmatrix}\equiv\phi_l^+(y-y_c), & \sigma=+1,\\ \begin{pmatrix}\phi_{l-1}(y-y_c)\\ \beta\phi_l(y-yc)\end{pmatrix}\equiv\phi_l^-(y-y_c), & \sigma=-1.\end{cases} \tag{13}$$

We will revive the original indices later. As such Eq. (9) can be cast in the following form:

$$\begin{aligned}\chi^0(\mathbf{r},\mathbf{r}';\omega)=\frac{1}{L_x^2}\sum_{k_xk_x'}\sum_{ll'}\sum_{\sigma\sigma'}\sum_{nn'}\Pi_{\substack{nn'\\ll'}}^{\sigma\sigma'}e^{iq_x(x'-x)}\\ \times\phi_{\sigma l}^*(y'-y_c)\phi_{\sigma'l'}(y'-y_c')\\ \times\phi_{\sigma'l'}^*(y-y_c')\phi_{\sigma l}(y-y_c)\\ \times\phi_n^*(z')\phi_{n'}(z')\phi_{n'}^*(z)\phi_n(z),\end{aligned} \tag{14}$$

where $y_c'=k_x'l_c^2$, $q_x=k_x'-k_x$ is the 1D momentum transfer, and

$$\Pi_{\substack{nn'\\ll'}}^{\sigma\sigma'}=\frac{1}{A_lA_{l'}}\Lambda_{\substack{nn'\\ll'}}^{\sigma\sigma'}. \tag{15}$$

Since the translational invariance persists in the x direction, we can Fourier transform this equation with respect to x. For this purpose, we multiply both sides of this equation by $e^{-iq_x'(x'-x)}$ and integrate over x'. The result, after a few straightforward mathematical steps, is

$$\chi^0(y,z;y',z';\omega) = \frac{1}{L_x}\sum_{k_x}\sum_{ll'}\sum_{\sigma\sigma'}\sum_{nn'}\Pi^{\sigma\sigma'}_{\substack{nn'\\ll'}} \times[\phi^*_{\sigma l}(y'-y_c)\phi_{\sigma' l'}(y'-y'_c)\phi^*_{\sigma' l'}(y-y'_c) \times\phi_{\sigma l}(y-y_c)]_{k'_x=k_x+q_x}\times\phi^*_n(z')\phi_{n'}(z') \times\phi^*_{n'}(z)\phi_n(z). \quad (16)$$

Though the specification $k'_x=k_x+q_x$ will be kept in mind, it will be omitted henceforth for the sake of brevity. Next, we recall that the induced particle density, employing Kubo's correlation function, is defined by[10]

$$n_{\rm in}(y,z;q_x,\omega) = \int dy'\chi^0(y,z;y',z';q_x,\omega)V(y',z';q_x,\omega), \quad (17)$$

where $V=V_{\rm ex}+V_{\rm in}$ is the total potential (energy), with $V_{\rm ex}$ ($V_{\rm in}$) as the external (induced) potential. Before we proceed further, it is important to note that while the system does observe a (physically) 2D translational invariance, the same is not true with the mathematical algorithm. As such, we are bound to make use of the so-called single-Fourier-transform components of $V(y,z;q_x,\omega)$ with respect to y to write

$$V(y,z;q_x,\omega) = \frac{1}{L_y}e^{iq_y y}V(z;q,\omega), \quad (18)$$

where $q=|\vec{q}|$, with $\vec{q}\equiv(q_x,q_y)$, and we introduce L_y just for the sake of keeping balance of the dimensions of the quantities involved in the problem. Now we seek the Fourier transform of Eq. (17) with respect to y. For this purpose, we multiply both sides of Eq. (17) by $e^{-iq_y y}$ and integrate over y. As such, we write, with the aid of Eqs. (17) and (18),

$$n_{\rm in}(z;q,\omega) = \frac{1}{L_y}\int dy\int dy' e^{-iq_y y}e^{-q_y y'} \times\int dz'\chi^0(y,z;y',z';q_x,\omega)V(z';q,\omega), \quad (19)$$

Eq. (19), with the aid of Eq. (16), assumes the following form:

$$n_{\rm in}(z;q,\omega) = \frac{1}{A}\sum_{k_x}\sum_{ll'}\sum_{\sigma\sigma'}\sum_{nn'}\Pi^{\sigma\sigma'}_{\substack{nn'\\ll'}} \times\int dy e^{-iq_y y}\phi^*_{\sigma' l'}(y-y'_c)\phi_{\sigma l}(y-y_c) \times\int dy' e^{iq_y y'}\phi^*_{\sigma l}(y'-y_c)\phi_{\sigma' l'}(y'-y'_c) \times\langle n|V(z';q,\omega)|n'\rangle\phi^*_{n'}(z)\phi_n(z), \quad (20)$$

where $A=L_xL_y$ stands for the area of the x-y plane. Next, induced potential in terms of induced particle density is given by

$$V_{\rm in}(z;q,\omega) = \int dz' V_{ee}(q,z-z')n_{\rm in}(z';q,\omega), \quad (21)$$

where $V_{ee}(q,z-z')$ is the Fourier transform of the binary Coulombic interactions and is given by

$$V_{ee}(q,z-z') = \frac{2\pi e^2}{\epsilon_b q}e^{-q|z-z'|}, \quad (22)$$

where ϵ_b is the background dielectric constant of the medium in which the Q2DEG is embedded. Making use of Eqs. (20) and (22) in Eq. (21) yields

$$V_{\rm in}(z;q,\omega) = \frac{1}{A}V_q\sum_{k_x}\sum_{ll'}\sum_{\sigma\sigma'}\sum_{nn'}\Pi^{\sigma\sigma'}_{\substack{nn'\\ll'}} \times\int dy e^{-iq_y y}\phi^*_{\sigma' l'}(y-y'_c)\phi_{\sigma l}(y-y_c) \times\int dy' e^{iq_y y'}\phi^*_{\sigma l}(y'-y_c)\phi_{\sigma' l'}(y'-y'_c) \times\langle n|V(z'';q,\omega)|n'\rangle \times\int dz' e^{-q|z-z'|}\phi^*_{n'}(z')\phi_n(z'), \quad (23)$$

where $V_q=2\pi e^2/(\epsilon_b q)$. Let us once and for all bring in an important issue regarding the sum over k_x. It may sound surprising but simple substitutions and mathematical manipulations can prove it to be true that the integrals in the second and third lines of Eq. (23) are complex conjugates of each other and that finally *nothing* depends on k_x in the right-hand side of this equation. Thus one can simplify this sum over k_x before proceeding further. Of utmost concern is the fact that the values of k_x are restricted to the range

$$-\frac{L_y}{2l_c^2} < k_x < +\frac{L_y}{2l_c^2} \quad (24)$$

or, equivalently,

$$-\frac{L_x}{2} < x < +\frac{L_x}{2} \quad (25)$$

in order to ensure that the center of gyration lies within the box of length L_x. This means the sum over k_x simplifies such that

$$\sum_{k_x} = \frac{L_x}{2\pi}\int_{-L_y/2l_c^2}^{+L_y/2l_c^2} dk_x = \frac{L_xL_y}{2\pi l_c^2} = \frac{A}{2\pi l_c^2}. \quad (26)$$

Therefore, Eq. (23) assumes the following form:

$$V_{\rm in}(z;q,\omega) = \frac{V_q}{2\pi l_c^2}\sum_{ll'}\sum_{\sigma\sigma'}\sum_{nn'}\Pi^{\sigma\sigma'}_{\substack{nn'\\ll'}} \times\int dy e^{-iq_y y}\phi^*_{\sigma' l'}(y-y'_c)\phi_{\sigma l}(y-y_c) \times\int dy' e^{iq_y y'}\phi^*_{\sigma l}(y'-y_c)\phi_{\sigma' l'}(y'-y'_c)$$

$$\times\langle n|V(z'';q,\omega)|n'\rangle \times \int dz' e^{-q|z-z'|}\phi^*_{n'}(z')\phi_n(z'). \quad (27)$$

Now take the matrix elements of V_{in} between the states $|m\rangle$ and $|m'\rangle$ to write

$$\langle m|V_{\rm in}(z)|m'\rangle = \frac{V_q}{2\pi l_c^2}\sum_{ll'}\sum_{\sigma\sigma'}\sum_{nn'}\Pi^{\sigma\sigma'}_{\substack{nn'\\ll'}} \times \int dy e^{-iq_y y}\phi^*_{\sigma' l'}(y-y'_c)\phi_{\sigma l}(y-y_c) \times \int dy' e^{iq_y y'}\phi^*_{\sigma l}(y'-y_c)\phi_{\sigma' l'}(y'-y'_c) \times \langle n|V(z'')|n'\rangle F_{mm'nn'}(q), \quad (28)$$

where

$$F_{mm'nn'}(q) = \int dz \int dz' \phi^*_m(z)\phi_{m'}(z)e^{-q|z-z'|}\phi^*_{n'}(z')\phi_n(z'). \quad (29)$$

Equation (28) can be cast in the following form:

$$\langle m|V_{\rm ex}|m'\rangle = \sum_{nn'}\left[\delta_{mn}\delta_{m'n'} - C\sum_{ll'}\sum_{\sigma\sigma'}\Pi^{\sigma\sigma'}_{\substack{nn'\\ll'}} \times \int dy e^{-iq_y y}\phi^*_{\sigma' l'}(y-y'_c)\phi_{\sigma l}(y-y_c) \times \int dy' e^{iq_y y'}\phi^*_{\sigma l}(y'-y_c)\phi_{\sigma' l'}(y'-y'_c) \times F_{mm'nn'}(q)\right]\langle n|V|n'\rangle, \quad (30)$$

where $C=V_q/(2\pi l_c^2)=e^2/(\epsilon_b q l_c^2)$. Now, since $V_{\rm ex}$ and V are related through

$$V_{\rm ex}(z) = \int dz' \epsilon(z,z')V(z'), \quad (31)$$

we can deduce from Eq. (30) the elements of the nonlocal, dynamic dielectric function expressed as follows:

$$\epsilon_{mm'nn'} = \delta_{mn}\delta_{m'n'} - C\sum_{ll'}\sum_{\sigma\sigma'}\Pi^{\sigma\sigma'}_{\substack{nn'\\ll'}} \times \int dy e^{-iq_y y}\phi^*_{\sigma' l'}(y-y'_c)\phi_{\sigma l}(y-y_c) \times \int dy' e^{iq_y y'}\phi^*_{\sigma l}(y'-y_c)\phi_{\sigma' l'}(y'-y'_c) \times F_{mm'nn'}(q). \quad (32)$$

Now it is important to specify that in this work we are strictly concerned with the case of a narrow quantum well where only the lowest (electric) subband is occupied and we ignore any excited subband. It is expected to be quite a reasonable approximation for low electron densities (n_{2d}) and at low temperatures where most of the experiments are performed in these systems. That means that we are virtually interested in a purely 2DEG at very low temperature. This would then imply that the subband index $m=m'=n=n'=0$ and hence the z coordinate drops out of consideration and thence the factor $F_{mm'nn'}(q)=1$. In addition, we should then take $\epsilon_n=0$ in Eq. (4) [as well as in Eq. (8)]. Thus the generalized nonlocal, dynamic dielectric function for a 2DEG in the presence of an applied perpendicular magnetic field and the Rashba spin-orbit interactions takes, from Eq. (32), the following form:

$$\epsilon(q,\omega) = 1 - C\sum_{ll'}\sum_{\sigma\sigma'}\Pi^{\sigma\sigma'}_{ll'}\int dy e^{-iq_y y}\phi^*_{\sigma' l'}(y-y'_c)\phi_{\sigma l}(y-y_c) \times \int dy' e^{iq_y y'}\phi^*_{\sigma l}(y'-y_c)\phi_{\sigma' l'}(y'-y'_c), \quad (33)$$

where $\phi_{\sigma l}(y-y_c)\cdots$ are as defined in Eq. (13) and $\Pi^{\sigma\sigma'}_{ll'}$ as specified in Eqs. (10) and (15), but with the subband indices (n,n') ignored. The next step is to diagnose carefully the sum over σ and σ' and solve the relevant integrals in Eq. (33). The details of this mathematical procedure are relegated to Appendix A for the sake of continuity. The result is that Eq. (33) can be written in a compact and convenient form as follows:

$$\epsilon(q,\omega) = 1 - C\sum_{ll'}[\Pi^{++}_{ll'}M^{++}_{ll'} + \Pi^{+-}_{ll'}M^{+-}_{ll'} + \Pi^{-+}_{ll'}M^{-+}_{ll'} + \Pi^{--}_{ll'}M^{--}_{ll'}]. \quad (34)$$

The explicit expressions of $\Pi^{\sigma\sigma'}_{ll'}$ and $M^{\sigma\sigma'}_{ll'}$ are given in Appendix A. Thus for a 2DEG -—in the presence of an applied perpendicular magnetic field and the Rashba spin-orbit interactions—the magnetoplasmon excitations are furnished by searching the zeros of the nonlocal, dynamic dielectric function $\epsilon(q,\omega)$ in Eq. (34). It should be pointed out that the present problem of a Q2DEG with a finite magnetic field turns out to be a nonmatrix formulation, unlike the zero-field cases of quasi-2DEG[27] and quasi-1DEG.[28] A few other recent works on the zero-field case of intrasubband charge-density excitations[29] and intersubband spin-density excitations[30] in 2D systems with SOI are also noteworthy. In what follows, we will diagnose Eq. (34) and discuss some of its special limits for a few physical case studies.

A. Special limit of zero SOI (or $\alpha=0$)

In the special limit of $\alpha=0$, we have $D_l=0\Rightarrow\beta=0$, $A_l=A_{l'}=1$, and the eigenfunction and eigenenergy are given by Eqs. (7) and (8). Equation (7) also means that, in the definitions of $M^{\sigma\sigma'}_{ll'}$ (see Appendix A), we should retain only the terms such as $I_{l,l'}(q),\ldots$. This then implies that $M^{+-}_{ll'}=0=M^{-+}_{ll'}$, the term $M^{--}_{ll'}$ does not contribute either, $M^{++}=|I_{ll'}(q)|^2$, and

$$\Pi_{ll'}^{++} \equiv \Pi_{ll'}^{0} = \frac{f(\epsilon_l) - f(\epsilon_{l'})}{\epsilon_l - \epsilon_{l'} + \hbar\omega^*}, \tag{35}$$

in Eq. (34). Thus Eq. (34) now simplifies to the form

$$\epsilon(q,\omega) = 1 - \frac{e^2}{\epsilon_b q l_c^2} \sum_{ll'} \Pi_{ll'}^{0} |I_{ll'}(q)|^2. \tag{36}$$

Note that Eq. (36) is exactly identical to Eq. (1) of Das Sarma[32] for (his) structure factor (that accounts for the periodicity of the system) $S=1$. Moreover, if we further impose the limit of zero magnetic field in Eq. (36), the simple mathematical analysis leads us to obtain a standard relation for the 2D plasmon dispersion given by $\omega=\omega_p$, where $\omega_p = \sqrt{2\pi n_{2D} e^2 q/(\epsilon_b m^*)}$ is the 2D screened plasmon frequency (with $\omega \propto \sqrt{q}$).

B. Diagnosis of Eq. (36) at zero temperature

In the zero temperature limit, when the Fermi distribution function can be replaced by a Heaviside step function, a simple mathematical analysis leads us to write Eq. (36) in the form

$$\epsilon(q,\omega) = 1 - \frac{2\pi e^2 q}{\epsilon_b m^*} \frac{1}{2\pi l_c^2} \frac{1}{x} \sum_{\substack{l \\ m>-l}} \frac{m}{\omega^2 - (m\omega_c)^2} |I_{l,l+m}(q)|^2, \tag{37}$$

where $x=q^2 l_c^2/2$. Now before we proceed further it should be pointed out how the 2D charge density shows up in such magnetized systems as 2DEG, with or without the Rashba SOI. For a particular subband, the density of states in the absence of a magnetic field (i.e., $B=0$) is a step function due to the two dimensionality. This continuous function splits, in a finite magnetic field ($B \neq 0$), into a series of δ-function-like spikes separated from each other by $\hbar\omega_c$. The states thus condense into sharp Landau levels. Because no states are lost, as many states must be contained in such a δ-function-like Landau level as were originally on the surface between two Landau levels at $B=0$. The degree of degeneracy n_L of a Landau level is therefore given by $n_l = D_0 \hbar\omega_c$, where $D_0 = m^*/(\pi\hbar^2)$ is the density of the subbands at $B=0$. However, this density must take into account the lifting of the spin degeneracy in the presence of a magnetic field and hence we should now have $D_0^* = m^*/(2\pi\hbar^2)$. The degeneracy of a Landau level is therefore given by $n_l = D_0^* \hbar\omega_c = 1/(2\pi l_c^2)$.

If the Landau state lies at an energy below the Fermi level, then at sufficiently low temperature it is occupied by exactly n_L electrons. A variation of an applied magnetic field then alters both the energy splitting and the degree of degeneracy of each level. To conclude with, in the present physical situation (of zero temperature) the 2D charge density is reasonably defined by $n_{2d}=n_L=1/(2\pi l_c^2)$. As such, Eq. (37) assumes the following form:

$$\epsilon(q,\omega) = 1 - \frac{\omega_p^2}{x} \sum_{\substack{l \\ m>-l}} \frac{m}{\omega^2 - (m\omega_c)^2} |I_{l,l+m}(q)|^2. \tag{38}$$

In the lowest-order approximation [i.e., $y=ql_c \ll 1$, see Eq. (B5) in Appendix B], Eq. (38) can be found to have the following solutions:

$$\omega^2 = \omega_{MP}^2 = \omega_p^2 + \omega_c^2 \tag{39}$$

and

$$\omega = \omega_B = j\omega_c, \quad j = 2,3,4, \ldots, \tag{40}$$

where ω_{MP} is the usual magnetoplasmon mode and ω_B is the well-known Bernstein mode that carries negligible spectral weight.[10]

C. Diagnosis of Eq. (34) at zero temperature

Equation (34) is the generalized nonlocal, dynamic dielectric function to include not only the applied magnetic field but also the Rashba spin-orbit interaction. The complexity of the analytical expression prevents us to diagnose this equation unlike the zero-SOI case discussed in Sec. II B. However, a thoughtful look at the single-particle energies [Eq. (4)] appearing in the denominator of each term in Eq. (34) leads us to deduce semi-empirical rules which turn out to be unfailingly true and substantiate exactly all the resonant (or Bernstein) modes in the magnetoplasmon spectrum in the presence of the Rashba SOI. Since we decide to work in terms of normalized frequency $\Omega=\omega/\omega_c$, we introduce an integer $n=\mathrm{Int}(\Omega)$, which refers to the cutoff (or maximum) value of Ω taken in the computation. We define a dimensionless frequency

$$\xi(n) = \left[\left(\frac{\epsilon_0}{\hbar\omega_c} \right)^2 + 2n \left(\frac{\alpha}{\hbar\omega_c l_c} \right)^2 \right]^{1/2}. \tag{41}$$

Now let us define another integer m, which stands for the cyclotron harmonics (i.e., $\omega=m\omega_c$). The semiempirical rules substantiate any resonant mode in the vicinity of a given m. We find that there are *four* such rules and a given Bernstein mode in the spectrum is dictated by *one and only one* of them. These rules are as follows:

$$t^{++} = m + \xi(n) - \xi(n-m), \tag{42}$$

$$t^{--} = m - \xi(n) + \xi(n-m), \tag{43}$$

$$t^{+-} = (m+1) - \xi(n) - \xi(n-m-1), \tag{44}$$

$$t^{-+} = (m-1) + \xi(n) + \xi(n-m+1). \tag{45}$$

It is evident from these equations that the resonant (or Bernstein) modes in the presence of Rashba SOI take place at the *noninteger* values, unlike the zero-SOI case. In addition, the quantities $t^{+-}\cdots$ are observed to strictly obey the relationship given by $t^{+-} < t^{--} < t^{++} < t^{-+}$. Here t^{++} (t^{--}) defines the *nearest* upper (lower) resonant mode in the vicinity of m and both are equidistant from m. In other words, the nearest resonant modes are shifted (from $m\Omega$) by

$$\Delta(m) = \frac{1}{2}(t^{++} - t^{--}) = \pm[\xi(n) - \xi(n-m)]. \quad (46)$$

For $\alpha=0$, these rules reproduce the resonant modes occurring at the cyclotron harmonics, just as expected. For example, $t^{++}=t^{+-}=t^{-+}=t^{--}=m$ and $\Delta(m)=0$, for $\alpha=0$, where $\xi(n)=\xi_0=1/2$. We will recall these rules while discussing our illustrative numerical examples on the magnetoplasmon dispersion in the following section.

D. On the variation of n_{2D} and B

In Sec. II B we have discussed how the 2D charge density is related to the strength of an applied magnetic field. Here we bring up the issue of the variation of the field strength B. With increasing field strength, the Landau states move to a higher energy, finally rising above the Fermi level ϵ_F. They are thereby emptied, and the excess electrons find a place in the next lower Landau level (possible because of the increased density of states). At sufficiently low temperature the Fermi level is very sharp, and the system then has its lowest free energy if a Landau level has just crossed the Fermi level. With still increasing B field, the free energy rises until the next Landau level is emptied. This leads to oscillations of the free energy as a function of an applied magnetic field. A variety of the oscillatory effects (see, for instance, Sec. I) result from this.

The aforesaid picture is particularly relevant to the study of the magnetotransport in the 2DEG, both with and without the Rashba SOI. As to the study of the magnetoplasmons in such a system, we assume that the moderate variation of the B field (n_{2D}) keeping the n_{2D} (B field) fixed does not alter the system drastically and provides us with the relevant information on the magnetoplasmon energy. In view of this, we will study the influence of the variation of the magnetic field B, the 2D charge density n_{2D}, and the Rashba parameter α on the oscillatory behavior and the resonance splittings of the magnetoplasmons in the system at hand.

III. ILLUSTRATIVE EXAMPLES ON MAGNETOPLASMON EXCITATIONS

This section is devoted to discuss our illustrative numerical examples on the magnetoplasmon excitations in a 2DEG in the presence of the Rashba spin-orbit interactions, computed at $T=0$ K. We do so by examining the influence of several parameters involved in the analytical results. These are, for instance, the Rashba parameter α, the 2D charge density n_{2D}, and the magnetic field B. The material parameters used are: effective mass $m^*=0.042m_0$, electron g factor $g=2.0$, Bohr magneton $\mu_B=0.9273\times10^{-20}$ erg/Gauss, background dielectric constant $\epsilon_b=13.9$, Rashba parameter $\alpha=1.6\times10^{-11}$ eV m, and the 2D charge density $n_{2D}=1.0\times10^{11}$ cm^{-2} as appropriate for $In_{1-x}Ga_xAs$, until and unless stated otherwise. For the sake of comparison, we will also present the numerical results without the Rashba SOI (i.e., with $\alpha=0$).

A. Magnetoplasmon dispersion without SOI (i.e., $\alpha=0$)

Figure 2 illustrates the dielectric function $\epsilon(q,\omega)$ as a function of the reduced frequency ω/ω_c, for the given values of n_{2D}, B, x, and α. This figure clearly demonstrates that, in the absence of an SOI, the resonant frequencies occur exactly at the cyclotron harmonics (i.e., $\omega=m\omega_c$) and the dielectric function observes an isolated singularity at each and every value of m (with $m=1,2,3,\ldots$). Physically speaking, this figure tells us something more than just the cyclotron harmonics: the arrows indicate where the real dielectric function becomes zero. These values are given by $\omega/\omega_c=1.102$, 2.232, 3.697, and 4.904. To be succinct, these should be the actual magnetoplasmon frequencies for the corresponding parameters. We will recall these frequencies and their meaning in the discussion of Fig. 4 and see that this really is the case.

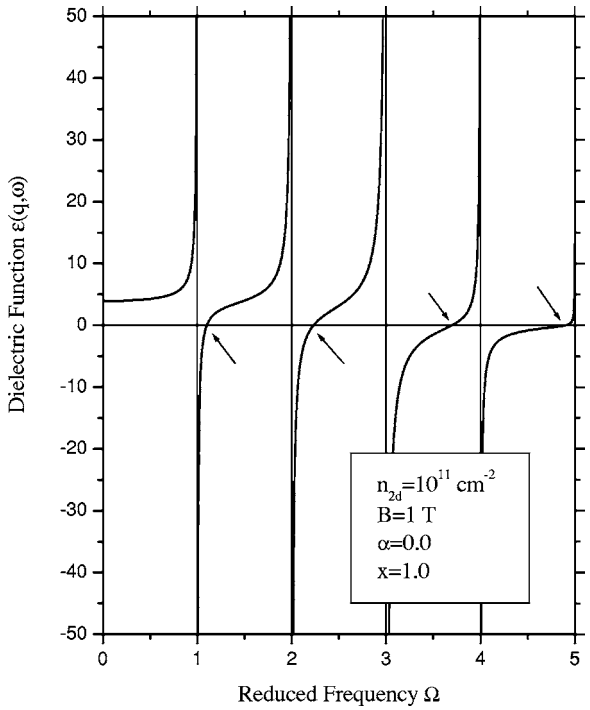

FIG. 2. Dielectric function $\epsilon(q,\omega)$ as a function of the reduced frequency ω/ω_c, for the given values of n_{2D}, B, α, and x. Here we take $\alpha=0$ in order to exclude the Rashba SOI. The parameters are as given inside the picture.

Figure 3 depicts the dielectric function $\epsilon(q,\omega)$ as a function of the reduced wave vector $y=ql_c$, for the given values of n_{2D}, B, α, and ω/ω_c. The solid and dashed curves referring, respectively, to $\omega/\omega_c=1.9$ and 1.5 cross the zero only for the two values of y, whereas the dotted curve for $\omega/\omega_c=1.1$ becomes zero for several values of y in the whole range. That means that the dielectric function with the lowest frequency should provide us with several magnetoplasmon frequencies for the corresponding set of parameters. This will also be reaffirmed while discussing the results in Fig. 4. It should be pointed out here that the observed oscillations in the dielectric function are an outright consequence of the Laguerre polynomial involved in the analytical results (see, for instance, Appendix B). Note how the amplitude of the oscillations diminishes with increasing y. We have noticed that such simple characteristics of the dielectric function as shown in Figs. 2 and 3 help us understand the magnetoplasmon dispersion to be discussed in what follows.

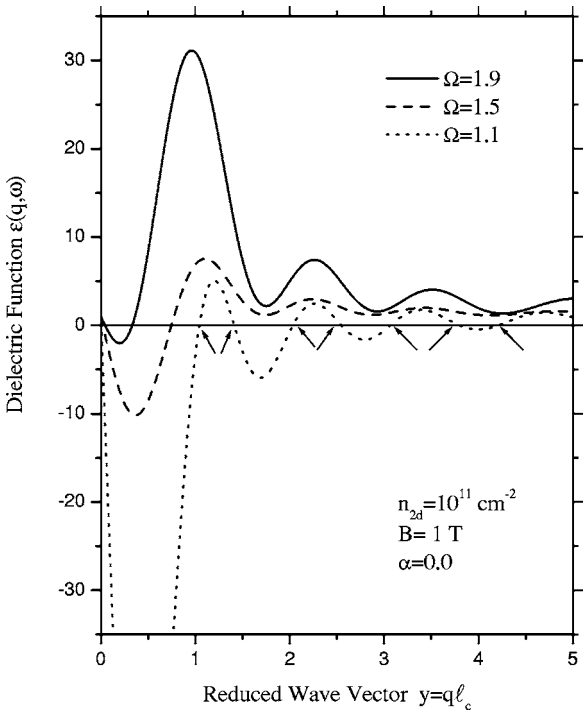

FIG. 3. Dielectric function $\epsilon(q,\omega)$ as a function of the reduced wave vector $y=ql_c$, for the given values of n_{2D}, B, α, and $\Omega=\omega/\omega_c$. Here we take $\alpha=0$ in order to exclude the Rashba SOI. The solid, dashed, and dotted curves refer, respectively, to $\omega/\omega_c=1.9$, 1.5, and 1.1. The parameters are as given inside the picture.

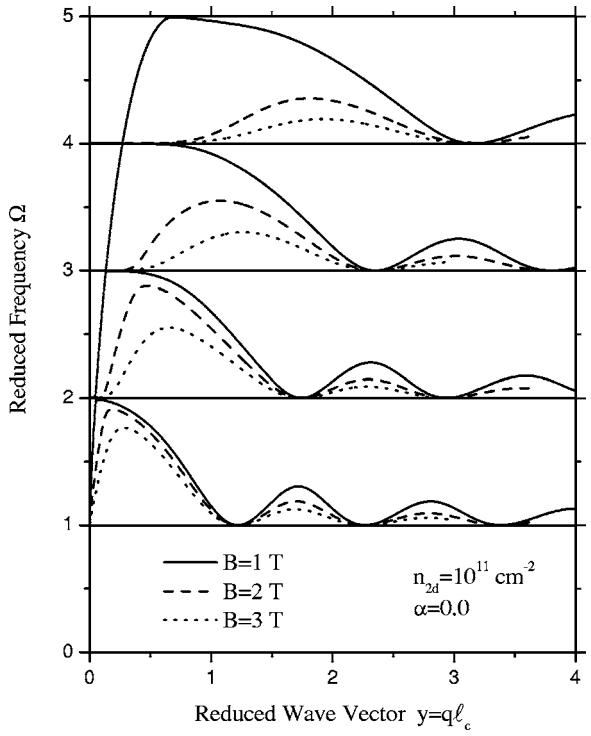

FIG. 4. Magnetoplasmon dispersion plotted as reduced frequency $\Omega=\omega/\omega_c$ versus reduced wave vector $y=ql_c$, for the given values of n_{2D}, B, and α. We take $\alpha=0$ in order to exclude the Rashba SOI. The solid, dashed, and dotted curves stand, respectively, for the magnetic field $B=1$, 2, and 3 T. The parameters are as given inside the picture.

Figure 4 shows the magnetoplasmon dispersion for the 2DEG without the Rashba spin-orbit interaction. The plot is rendered in terms of the dimensionless energy $\Omega=\omega/\omega_c$ and the wave vector $y=ql_c$. Just as dictated by Fig. 2, the resonant (or Bernstein) modes occur at the exact cyclotron harmonics defined by $\omega=m\omega_c$. This figure also affirms the oscillatory behavior of the magnetoplasmon dispersion as a function of y in the short wavelength limit. The magnetoplasmon dispersion, for any value of the magnetic field, is clearly describable as follows. As the wave vector y increases, the frequency ω increases until it reaches its maximum value (slightly below the next higher harmonics) and then decreases gradually. As y becomes sufficiently large, ω comes closer to the next lower harmonics and oscillates. The amplitude of the oscillations diminishes with increasing y, just as it is expected. As the magnetic field is increased, the amplitude of the magnetoplasmon oscillation decreases. This is a standard textbook notion: the higher the magnetic field, the lower the radius of the cyclotron orbits. At the higher energy, the amplitude (period) of the oscillations becomes smaller (larger) and the center of the oscillations gradually shifts towards the higher values of y. This seems to be an artifact of the cyclotron energy playing a lesser role at the higher energy. It is observed that at a very large value of y, the magnetoplasmon mode becomes asymptotic to the resonant mode at the respective harmonics. Also observed is the fact that if we draw a vertical line at $y=\sqrt{2}$ (i.e., $x=1$), then this line crosses the curve for $B=1$ T at exactly the frequencies indicated by the arrows in Fig. 2. Similarly, if we draw a horizontal line at $\Omega=1.1$, we see that it cuts the curve for $B=1$ T at exactly the values of y indicated by the arrows in Fig. 3. This confirms the strategy that the (analytic) zeros of the dielectric function stands for the magnetoplasmon frequencies for the respective set of parameters.

Figure 5 illustrates the magnetoplasmon resonance splittings in the long wavelength limit in the vicinity of the second harmonics (with $m=2$). The resonance splittings are seen to give rise to a gap in the magnetoplasmon spectrum. We measure the gap between the bottom of the upper curve and the top of the lower curve. One can see that the magnitude of the gap becomes larger with increasing magnetic field. Here the gap is defined by $\Delta=0.0303$, 0.4738, and 1.917 meV, respectively, for $B=1$, 2, and 3 T. It should be pointed out that the lower (upper) curves of Fig. 4, with reference to $\omega=2\omega_c$, and the lower (upper) curves of Fig. 5 are the two limits of the same respective curves. With increasing magnetic field, the bottom (top) of the upper (lower) curves shifts towards higher values of y because we have normalized the propagation vector q by multiplying with the magnetic length l_c. It should be emphasized that such splittings are found only for $m\geqslant 2$ and no splitting is found for $m=1$. We expect that such long wavelength energy gaps in the magnetoplasmon dispersion as shown here must have some important consequences on the magnetotransport in the 2DEG.

B. Magnetoplasmon dispersion with SOI (i.e., $\alpha\neq 0$)

Figure 6 illustrates the dielectric function $\epsilon(q,\omega)$ as a function of the reduced frequency ω/ω_c, for the given values

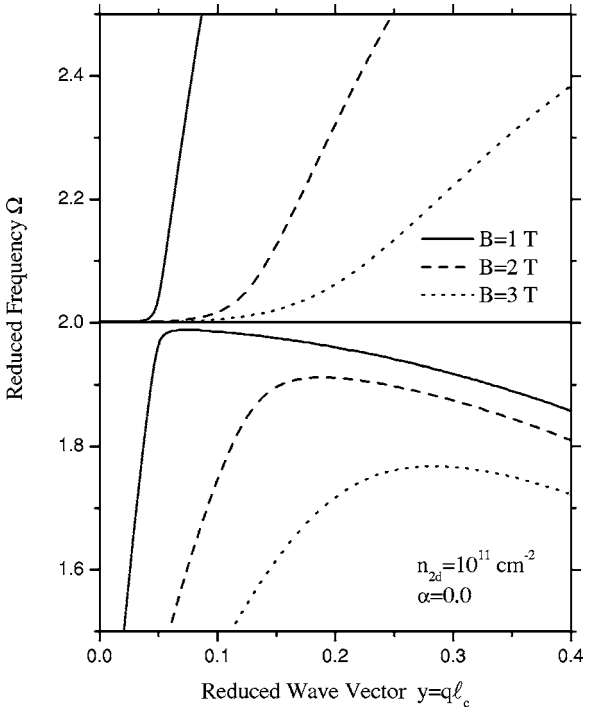

FIG. 5. The same as in Fig. 4, but showing the magnetoplasmon resonance splittings at the second cyclotron harmonics ($\omega=2\omega_c$) in the long wavelength limit. The parameters are as given inside the picture.

of n_{2D}, B, α and x. This figure clearly demonstrates that, in the presence of the Rashba SOI, the resonant frequencies do not occur at the cyclotron harmonics and the dielectric function observes the isolated singularities at noninteger values [$\omega=(m\pm x_0)\omega_c$, with $m=1,2,3,\ldots$]. This figure speaks much different from Fig. 2 in that the nearest resonant modes (indicated by the arrows) are equidistant from any and every value of m. In addition, there are also next-nearest resonant modes which occur at $\omega=(m+y_0)\omega_c$, with $y_0(\neq x_0)\gtrless 0$. That this really is the case will be confirmed through the computation of the magnetoplasmon dispersion as a function of the propagation vector in Fig. 8 (see below). However, as regards the actual magnetoplasmon frequencies, these are (and should, in principle, be) still given by the analytic zeros of the real dielectric function.

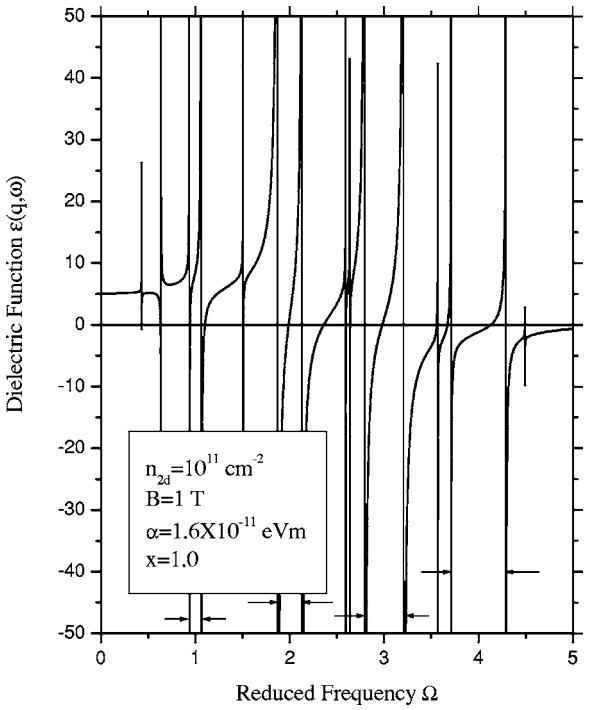

FIG. 6. Dielectric function $\epsilon(q,\omega)$ as a function of the reduced frequency $\Omega=\omega/\omega_c$, for the given values of n_{2D}, B, α, and x. Contrary to Fig. 2, here we take $\alpha\neq 0$ in order to include the Rashba SOI. The parameters are as given inside the picture.

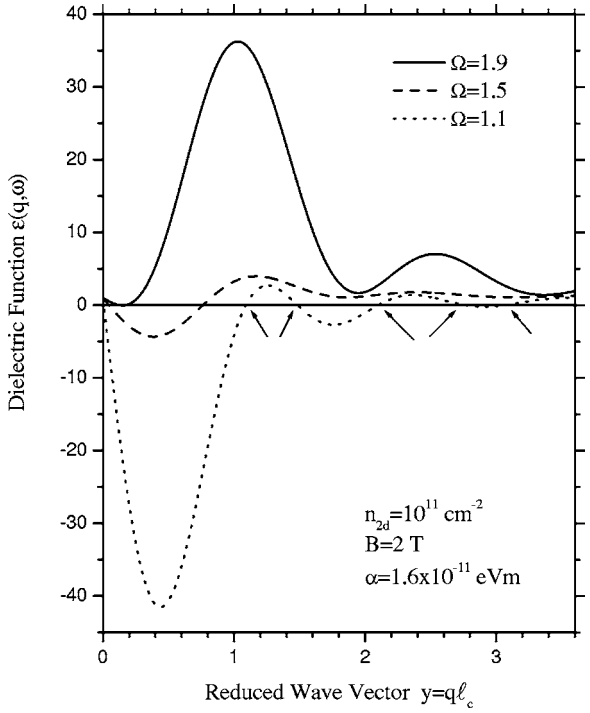

FIG. 7. Dielectric function $\epsilon(q,\omega)$ as a function of the reduced wave vector $y=ql_c$, for the given values of n_{2D}, B, α, and ω/ω_c. Here we take $\alpha\neq 0$ in order to include the Rashba SOI. The solid, dashed, and dotted curves refer, respectively, to $\Omega=1.9$, 1.5, and 1.1. The parameters are as given inside the picture.

Figure 7 depicts the dielectric function $\epsilon(q,\omega)$ as a function of the reduced wave vector $y=ql_c$, for the given values of n_{2D}, B, α, and Ω. The solid curve referring to $\Omega=1.9$ barely touches the zero of the dielectric function and the dashed curve for $\Omega=1.5$ crosses the zero only for the two values of y. The dotted curve for $\Omega=1.1$ becomes zero for several values of y in the whole range. That means that the dielectric function with the lowest frequency should provide us with several magnetoplasmon frequencies for the corresponding set of parameters. Again, the observed oscillations in the dielectric function are an outright consequence of the associated Laguerre polynomial involved in the analytical results (see, for instance, Appendix B). Just as in Fig. 3, the amplitude of the oscillations diminishes with increasing y. The values of y indicated by the arrows, for $\Omega=1.1$, read $y=1.0907$, 1.4845, 2.0996, 2.7693, and 3.0651. We will see in the magnetoplasmon dispersion (see Fig. 8) how these values

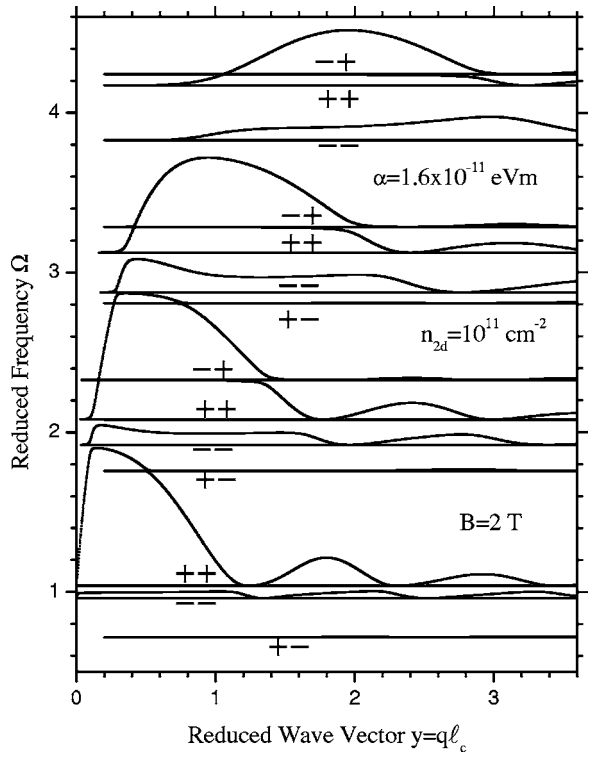

FIG. 8. Magnetoplasmon dispersion displayed as reduced frequency $\Omega=\omega/\omega_c$ versus reduced wave vector $y=ql_c$, for the given values of n_{2D}, B, and α. We take $\alpha\neq 0$ in order to include the Rashba SOI. To let the picture speak clearly, we plot the dispersion only for a single value of $B=2$ T. The curves labeled as $+-\cdots$ refer to the dimensionless frequencies represented by $t^{+-}\cdots$ [see Eqs. (42)–(45)]. The parameters are as given inside the picture.

of y correspond exactly to the frequency $\omega/\omega_c=1.1$.

Figure 8 shows the magnetoplasmon dispersion for the 2DEG with the Rashba spin-orbit interaction included. The plot is rendered in terms of the dimensionless energy $\Omega=\omega/\omega_c$ and the propagation vector $y=ql_c$. Just as dictated by Fig. 7, the resonant (or Bernstein) modes occur at the noninteger values defined by $\omega=(m\pm x_0)\omega_c$ and $\omega=(m+y_0)\omega_c$, with $y_0\gtrless 0$. The former (latter) stands for the nearest (next-nearest) resonant modes. There are numerous interesting features this figure reveals about the effect of the Rashba SOI on the magnetoplasmon excitations in the 2DEG. For instance, (1) the oscillatory behavior of the magnetoplasmons in the SWL, (2) the existence of the resonant modes at the noninteger values, unlike the zero SOI case, (3) the resonance splittings may occur not only in the LWL, but also in the SWL (see, e.g., the splittings at $y=1.353$, 1.979, and 2.918 all taking place slightly below the resonant modes marked as $-+$ above $m=2$, 3, and 4), (4) some narrow but finite resonance splittings can also exist around $m=1$, particularly in the SWL, unlike the zero SOI case, (5) all the magnetoplasmons start and propagate just above a certain resonant mode… . It is noticed that at very large value of y, every magnetoplasmon mode becomes asymptotic to the respective resonant mode. As the magnetic field is increased, the amplitude of the magnetoplasmon oscillations decreases, just as before in the zero SOI case. As y becomes sufficiently large, the magnetoplasmon modes come closer to the next lower resonant modes and oscillate. Again, the amplitude of the oscillations diminishes with increasing y, just as in the zero SOI case (see Fig. 4). The rest of the discussion related to the propagation characteristics of the magnetoplasmons in the LWL related with Fig. 4 is still valid. It is observed that if we draw a horizontal line at $\Omega=1.1$, it cuts the magnetoplasmon mode at exactly the values of y indicated by the arrows in Fig. 7.

Figure 9 illustrates the magnetoplasmon resonance splittings in the long wavelength limit in the vicinity of the second harmonics (with $m=2$) in the presence of Rashba SOI, with different values of the magnetic field B. We have shown the resonance splittings just below the nearest resonant modes ($++$ and $--$, see Fig. 8). It is observed that the $++$ ($--$) resonant modes are shifted towards lower (higher) energy with increasing magnetic field. On the other hand, the magnetoplasmon modes move towards lower energy (below both the nearest resonant modes) with increasing magnetic field. These resonance splittings give rise to the gaps in the magnetoplasmon spectrum. For the set of parameters used, the measured gaps below the $++$ resonant modes are defined by $\Delta=0.193$, 0.413, and 0.619 meV, respectively, for $B=2.0$, 2.5, and 3.0 T. With the same token, the magnitude of the gaps below the $--$ resonant modes are given by $\Delta=0.226$, 0.379, and 0.793 meV, respectively, for $B=2.0$, 2.5, and 3.0 T. In general, the magnitude of the gaps becomes larger with increasing magnetic field. Some other resonance splittings of smaller magnitude at higher energy, which correspond to the highest $(-+)$ resonant mode (associated with $m=2$) in Fig. 8, are also noteworthy.

Figure 10 illustrates the magnetoplasmon resonance splittings in the long wavelength limit in the vicinity of the second harmonics (with $m=2$) in the presence of Rashba SOI, with different values of the 2D charge density n_{2D}. Again, the resonance splittings are shown just below the nearest resonant modes ($++$ and $--$, see Fig. 8). It is observed that no resonant mode is shifted in energy because of the variation of the charge density. This is simply because the 2D charge density does not appear in the single-particle energies [see, e.g., Eq. (4)]; it is only implicitly involved in the numerator outside the sum in the second term of the generalized dielectric function in Eq. (34). As such, it is not difficult to understand that the variation in n_{2D} should affect only the collective (magnetoplasmon) modes in the system. With decreasing charge density, the magnetoplasmon modes (below both $++$ and $--$ resonant modes) are shifted towards lower energies thereby increasing the magnitude of the existing gaps in the excitation spectrum. For the set of parameters used, the measured gaps below the $++$ resonant modes are defined by $\Delta=0.149$, 0.209, and 0.281 meV, respectively, for $n_{2D}=1.2\times10^{11}$ cm^{-2}, 1.0×10^{11} cm^{-2}, and 0.8×10^{11} cm^{-2}. Similarly, the magnitude of the gaps below the $--$ resonant modes are given by $\Delta=0.094$, 0.111, and 0.187 meV, respectively, for $n_{2D}=1.2\times10^{11}$, 1.0×10^{11}, and 0.8×10^{11} cm^{-2}. In general, the size of the gaps becomes larger with decreasing 2D charge density. Other resonance splittings of lesser magnitude seen at higher energy are those which correspond to the highest $(-+)$ resonant mode (associated with $m=2$ in Fig. 8).

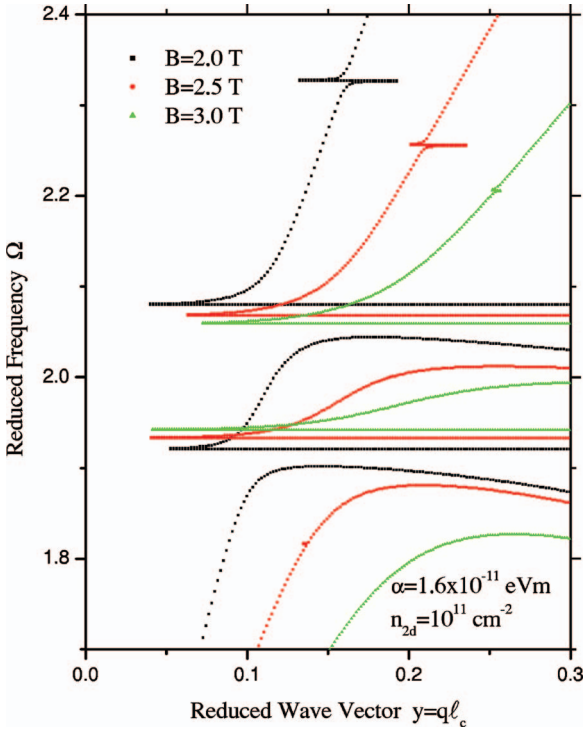

FIG. 9. (Color) Magnetoplasmon resonance splittings shown as reduced frequency $\Omega=\omega/\omega_c$ versus reduced wave vector $y=ql_c$ in the LWL, for the given values of B. We call attention to the effect of varying the magnetic field on the resonance splittings. The other parameters are as given inside the picture.

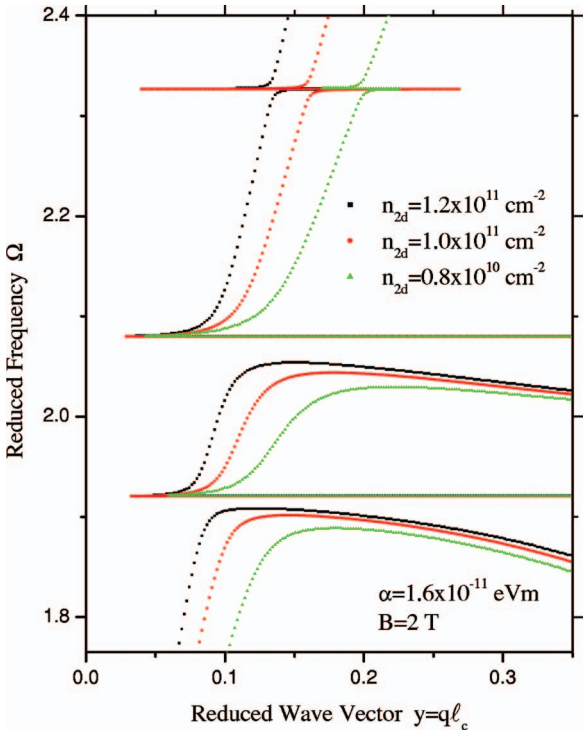

FIG. 10. (Color) Magnetoplasmon resonance splittings shown as reduced frequency $\Omega=\omega/\omega_c$ versus reduced wave vector $y=ql_c$ in the LWL, for the given values of charge density n_{2D}. We call attention to the effect of varying the 2D charge density on the resonance splittings. The other parameters are as given inside the picture.

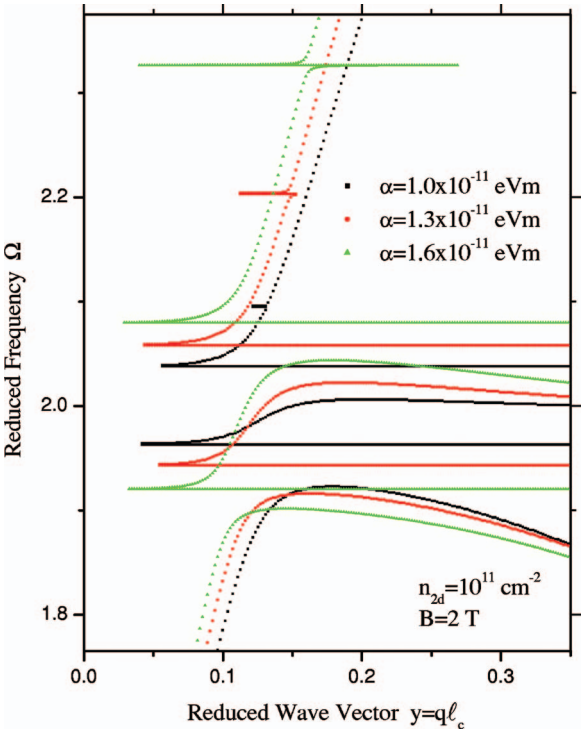

FIG. 11. (Color) Magnetoplasmon resonance splittings shown as reduced frequency $\Omega=\omega/\omega_c$ versus reduced wave vector $y=ql_c$ in the LWL, for the given values of the Rashba parameter α. We call attention to the effect of varying the Rashba parameter on the resonance splittings. The other parameters are as given inside the picture.

Figure 11 illustrates the magnetoplasmon resonance splittings in the long wavelength limit in the vicinity of the second harmonics (with $m=2$) in the presence of Rashba SOI, with different values of the Rashba parameter α. The resonance splittings are only shown just below the nearest resonant modes ($++$ and $--$, see Fig. 8). It is observed that the $++$ ($--$) resonant modes are shifted towards higher (lower) energy with increasing α. On the other hand, the magnetoplasmon modes above (below) the $--$ resonant modes are, in general, seen to be shifted towards higher (lower) energy with increasing α. For the set of parameters used, the measured gaps below the $++$ resonant modes are defined by $\Delta=0.182$, 0.198, and 0.204 meV, respectively, for $\alpha=1.0\times10^{-11}$, 1.3×10^{-11}, and 1.6×10^{-11} eV m. Similarly, the magnitude of the gaps below the $--$ resonant modes are found to be $\Delta=0.204$, 0.165, and 0.101 meV, respectively, for $\alpha=1.0\times10^{-11}$, 1.3×10^{-11}, and 1.6×10^{-11} eV m. In general, the gap becomes larger (smaller) below the $++$ ($--$) resonant mode with increasing Rashba parameter. Other weaker resonance splittings seen at higher energy are those which correspond to the highest ($-+$) resonant mode for the respective value of α.

C. Inverse dielectric function $\epsilon^{-1}(q,\omega)$

The literature is a live example that spintronics is richer in semiconductors than in metals because doping, gating, and heterojunction formation can be exploited to tailor the key

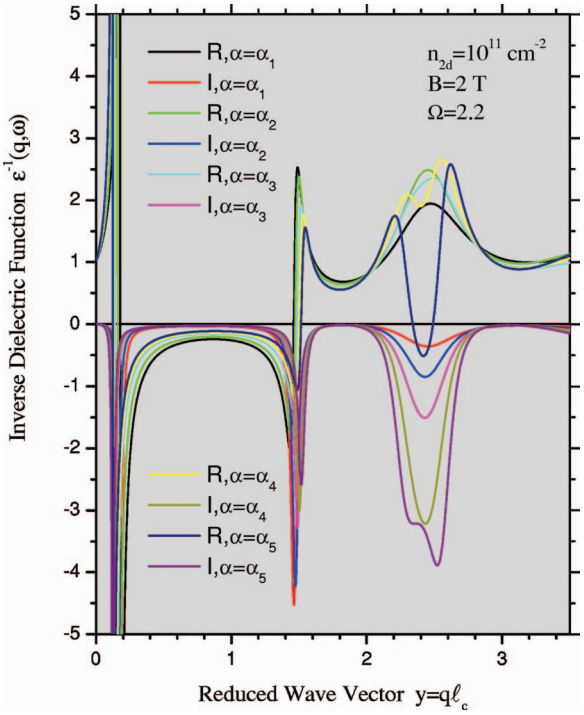

FIG. 12. (Color) Inverse dielectric function $\epsilon^{-1}(q,\omega)$ versus reduced wave vector $y=ql_c$, for the given values of the Rashba parameter α. The symbol R (I) refers to real (imaginary) part of the dielectric function. Here $\alpha_1=0.5\times10^{-11}$ eV m, $\alpha_2=1.0\times10^{-11}$ eV m, $\alpha_3=1.5\times10^{-11}$ eV m, $\alpha_4=1.7\times10^{-11}$ eV m, and $\alpha_5=1.9\times10^{-11}$ eV m. The other parameters are as given inside the picture.

material properties and because of the intimate relationship between optical and transport properties in semiconductors. In view of this, we also studied briefly the inverse (nonlocal, dynamic) dielectric function $[\epsilon^{-1}(q,\omega)]$, which is closely related to the longitudinal and transverse (Hall) resistance in such 2D electron systems. For instance, the longitudinal (Hall) resistance ρ_{xx} (ρ_{xy}) is determined by the imaginary (real) part of the inverse dielectric function. Such an investigation is worthwhile because it would allow us to use the transport measurements to probe the reactive (real) part of the inverse dielectric function.

Figure 12 illustrates the inverse dielectric function $\epsilon^{-1}(q,\omega)$ as a function of the reduced wave vector $y=ql_c$, for the given values of the Rashba parameter α. It should be pointed out that the quantity that directly affects the transport is the spectral weight $\mathrm{Im}[\epsilon^{-1}(q,\omega)]$, which contains both the single-particle contribution at large q and the collective (magnetoplasmon) contribution at small q. It is clearly observed that the sharp peaks at the reduced wave vector $y=0.178$ and 1.456 stand for the magnetoplasmon modes for the given frequency $\Omega=2.2$ (see, e.g., Fig. 8) and the broader peak at $y\simeq2.429$ refers to the single-particle excitations (when the magnetoplasmons almost merge with the resonant modes). Clearly, these peaks are a result of the existing poles of the inverse dielectric function at the corresponding values of ω and q. Due to Rashba spin splitting, there are four different momentum transfers for a given frequency Ω: two intra $(++$ and $--)$ and two inter $(+-$ and $-+)$ spin-channel transitions. This gives rise to the fine structures in both the real and imaginary parts of $\epsilon^{-1}(q,\omega)$. These fine structures are, however, vividly resolved only when the Rashba parameter α characterizing the SOI is sufficiently large. In the present situation such structures are seen, for instance, for $\alpha=1.7\times10^{-11}$ and 1.9×10^{-11} eV m.

We believe that such fine structures should also be mimicked in the plots of the longitudinal (ρ_{xx}) and transverse (ρ_{xy}) resistances plotted as a function of frequency. It is noteworthy that the quantity $\mathrm{Im}[\epsilon^{-1}(q,\omega)]$ also implicitly provides the details of the Raman (or electron) scattering cross-section $S(q)$ in the system.[13] Thus ρ_{xx} can also be understood as a weighted sum of the scattering cross section. As such, we expect that the main effect of the Rashba spin-splitting is to redistribute the scattering probability at different q but not to significantly change the total cross section summed over all q. Extensive details of the study of ρ_{xx} and ρ_{xy} are deferred to a future publication.

IV. CONCLUDING REMARKS

In summary, we have investigated extensively the magnetoplasmons in a 2DEG in the presence of the Rashba spin-orbit interactions in the framework of random-phase approximation. This includes the dielectric function versus the frequency and the propagation vector, magnetoplasmon excitation spectra, the resulting resonance splittings, both with and without the Rashba SOI. In particular, we have paid more attention to study the magnetoplasmon propagation in the presence of the Rashba SOI. The extensive study of the effects of the variation of the magnetic field B, 2D charge density n_{2D}, and the Rashba parameter α on the excitation spectrum leads us to draw the following conclusions. In the absence of the Rashba SOI, the magnetoplasmons oscillate just above the resonant (or Bernstein) modes specified by integer cyclotron harmonics ($\omega=m\omega_c$) in the SWL and the resonance splittings occur in the LWL. The magnitude of these splittings increase with increasing magnetic field B. In the presence of the Rashba SOI, the spin-splitting gives rise to *four* resonant modes in the vicinity of every harmonic m. These resonant modes have been specified by unfailingly true semiempirical rules. The magnetoplasmon modes now appear and oscillate above all the noninteger resonant modes in the SWL and the (most widely existing) nearest resonant splittings in the LWL have been analyzed. As such, the magnetoplasmon spectrum in the presence of the Rashba SOI happen to be complex and richer as compared to that with the zero SOI.

The nearest resonance splittings in the presence of the Rashba SOI are observed to obey the following tendencies. Both energy gaps due to the resonance splitting increase with the increasing magnetic field and decrease with increasing 2D charge density. While the upper nearest energy gap remains moderately invariant, the lower one decreases with increasing α. In the presence of the Rashba SOI, there are additional (weaker) resonance splittings occurring in the SWL. Plotting the full spectrum as a function of B and α separately, keeping the propagation vector fixed, reveals that the magnetoplasmon dispersion is sensitive and significant at

the higher (lower) values of α (B). This is understandable simply by having a careful look at the single-particle energy, Eq (4), which dictates the larger effect of the SOI at higher (lower) value of α (B).

Depending upon the set of parameters, the existing gaps in the magnetoplasmon spectrum due to the resonance splittings can be on the order of a few meV. This suggests the application of the Rashba spintronic systems as frequency modulators and/or filters that would prohibit the magnetoplasma waves at certain frequency while allow free propagation at others.

A brief study of the inverse dielectric function leads us to substantiate the magnetoplasmon modes searched with the zeros of the dielectric function. This is what we should expect because searching the zeros of the dielectric function and the poles of the inverse dielectric function must produce exactly identical results. In addition, studying the inverse dielectric function for the given values of α provides us with important and relevant information on the effect of the Rashba SOI on the longitudinal and Hall resistances. The imaginary part of the inverse dielectric function also provides us with significant estimates of the Raman (or electron) scattering cross section.

Finally, we believe that the present investigation of the magnetoplasmon excitation spectrum in a 2DEG in the presence of the Rashba spin-orbit interaction will prove to be useful for the scientific community involved in and excited with the emerging field of semiconductor spintronics. We hope that such behavior characteristics of the magnetoplasmons as studied and predicted here can be verified by, for example, the Raman (or inelastic light) scattering experiments. Currently, we have been studying the effect of the Rashba SOI on the charge-density excitations in a quasi-1DEG in the presence of a perpendicular magnetic field and the results will be reported shortly.

ACKNOWLEDGMENTS

This work was partially supported by CONACyT Grant No. SEP-2003-C02-42761. I have enjoyed some very fruitful discussions with Sergio Ulloa and Godfrey Gumbs.

APPENDIX A: THE DETAILS OF THE FACTORS OF $M_{ll'}^{\sigma\sigma'}$ IN EQ. (34)

First of all we revive the original indices [see Eq. (13)], perform carefully the multiplication of bra and ket type vectors, and integrate to evaluate various factors $M_{ll'}^{\sigma\sigma'}$ involved in Eq. (34) as follows:

$$M_{ll'}^{++} = \beta\beta^*\beta'\beta'^*|I_{l-1,l'-1}(q)|^2 + \beta\beta'^*I_{l-1,l'-1}(q)I_{l,l'}^*(q) + \beta^*\beta' I_{l,l'}(q)I_{l-1,l'-1}^*(q) + |I_{l,l'}(q)|^2, \tag{A1}$$

$$M_{ll'}^{+-} = \beta\beta^*|I_{l-1,l'-1}(q)|^2 + \beta\beta' I_{l-1,l'-1}(q)I_{l,l'}^*(q) + \beta^*\beta'^* I_{l,l'}(q)I_{l-1,l'-1}^*(q) + \beta'\beta'^*|I_{l,l'}(q)|^2, \tag{A2}$$

$$M_{ll'}^{-+} = \beta'\beta'^*|I_{l-1,l'-1}(q)|^2 + \beta^*\beta'^* I_{l-1,l'-1}(q)I_{l,l'}^*(q) + \beta\beta' I_{l,l'}(q)I_{l-1,l'-1}^*(q) + \beta\beta^*|I_{l,l'}(q)|^2, \tag{A3}$$

$$M_{ll'}^{--} = |I_{l-1,l'-1}(q)|^2 + \beta^*\beta' I_{l-1,l'-1}(q)I_{l,l'}^*(q) + \beta\beta'^* I_{l,l'}(q)I_{l-1,l'-1}^*(q) + \beta\beta^*\beta'\beta'^*|I_{l,l'}(q)|^2, \tag{A4}$$

where $\beta' = -iD_{l'}$ and the asterisk refers to the complex conjugate of the respective quantity. Furthermore, the simplified factors of the polarizabilty functions $\Pi_{ll'}^{\sigma\sigma'}$ involved in Eq. (34) [see Eqs. (10) and (15)] are defined as follows:

$$\Pi_{ll'}^{++} = \frac{1}{A_l A_{l'}} \frac{f(\epsilon_l^+) - f(\epsilon_{l'}^+)}{\epsilon_l^+ - \epsilon_{l'}^+ + \hbar\omega^*}, \tag{A5}$$

$$\Pi_{ll'}^{+-} = \frac{1}{A_l A_{l'}} \frac{f(\epsilon_l^+) - f(\epsilon_{l'}^-)}{\epsilon_l^+ - \epsilon_{l'}^- + \hbar\omega^*}, \tag{A6}$$

$$\Pi_{ll'}^{-+} = \frac{1}{A_l A_{l'}} \frac{f(\epsilon_l^-) - f(\epsilon_{l'}^+)}{\epsilon_l^- - \epsilon_{l'}^+ + \hbar\omega^*}, \tag{A7}$$

$$\Pi_{ll'}^{--} = \frac{1}{A_l A_{l'}} \frac{f(\epsilon_l^-) - f(\epsilon_{l'}^-)}{\epsilon_l^- - \epsilon_{l'}^- + \hbar\omega^*}. \tag{A8}$$

APPENDIX B: FOR INTEGRALS OF THE TYPE $I_{ll'}(q)$ ⋯IN APPENDIX A

The integrals of the type $I_{ll'}(q)$ ⋯in Appendix A are simplified to yield

$$I_{l,l'}(q) = \left(\frac{l!}{l'!}\right)^{1/2} e^{-x/2} e^{-iq_y k_x l_c^2} e^{-iq_y q_x l_c^2/2} \times \left[-\frac{l_c}{\sqrt{2}}(q_x + iq_y)\right]^{l'-l} L_l^{l'-l}(x), \tag{B1}$$

$$I_{l,l'}^*(q) = \left(\frac{l!}{l'!}\right)^{1/2} e^{-x/2} e^{+iq_y k_x l_c^2} e^{+iq_y q_x l_c^2/2} \times \left[-\frac{l_c}{\sqrt{2}}(q_x - iq_y)\right]^{l'-l} L_l^{l'-l}(x), \tag{B2}$$

$$I_{l-1,l'-1}(q) = \left(\frac{(l-1)!}{(l'-1)!}\right)^{1/2} e^{-x/2} e^{-iq_y k_x l_c^2} e^{-iq_y q_x l_c^2/2} \times \left[-\frac{l_c}{\sqrt{2}}(q_x + iq_y)\right]^{l'-l} L_{l-1}^{l'-l}(x), \tag{B3}$$

$$I^{*}_{l-1,l'-1}(q) = \left(\frac{(l-1)!}{(l'-1)!}\right)^{1/2} e^{-x/2} e^{+iq_y k_x l_c^2} e^{+iq_y q_x l_c^2/2} \times \left[-\frac{l_c}{\sqrt{2}}(q_x - iq_y)\right]^{l'-l} L_{l-1}^{l'-l}(x), \tag{B4}$$

where $x=q^2l_c^2/2$ and $L_n^m(x)$ is an associated Laguerre polynomial[31] defined by

$$L_n^m(x) = \frac{1}{n!} e^x x^{-m} \frac{d^n}{dx^n}(e^{-x} x^{n+m}).$$

Thus the integrals involved in Eqs. (A1)–(A4) take the following forms (with $l<l'$):

$$|I_{l,l'}(q)|^2 = \frac{l!}{l'!} e^{-x} x^{l'-l} [L_l^{l'-l}(x)]^2, \tag{B5}$$

$$|I_{l-1,l'-1}(q)|^2 = \left(\frac{l'}{l}\right) \frac{l!}{l'!} e^{-x} x^{l'-l} [L_{l-1}^{l'-l}(x)]^2, \tag{B6}$$

$$I_{l-1,l'-1}(q) I^{*}_{l,l'}(q) = \left(\frac{l'}{l}\right)^{1/2} \frac{l!}{l'!} e^{-x} x^{l'-l} L_{l-1}^{l'-l}(x) L_l^{l'-l}(x), \tag{B7}$$

$$I_{l,l'}(q) I^{*}_{l-1,l'-1}(q) = \left(\frac{l'}{l}\right)^{1/2} \frac{l!}{l'!} e^{-x} x^{l'-l} L_l^{l'-l}(x) L_{l-1}^{l'-l}(x). \tag{B8}$$

Note that the right-hand sides of Eqs. (B5)–(B8) are all absolutely real quantities. We remind that Eqs. (B5)–(B8) confirm the statement made in the text following Eq. (23).

[1] G. Dresselhaus, Phys. Rev. **100**, 580 (1955).
[2] E. I. Rashba, Sov. Phys. Solid State **2**, 1109 (1960); Yu. A. Bychkov and E. I. Rashba, JETP Lett. **39**, 78 (1984); E. I. Rashba and Al. L. Efros, Phys. Rev. Lett. **91**, 126405 (2003).
[3] R. Winkler, *Spin-Orbit Coupling Effects in Two-Dimensional Electron and Hole Systems* (Springer, New York, 2003).
[4] For a recent review of the field of spintronics, see I. Zutic, J. Fabian, and S. Das Sarma, Rev. Mod. Phys. **76**, 323 (2004).
[5] S. Datta and B. Das, Appl. Phys. Lett. **56**, 665 (1990).
[6] B. E. Kane, Nature (London) **393**, 133 (1998).
[7] J. Nitta, F. E. Meijer, and H. Takayanagi, Appl. Phys. Lett. **75**, 695 (1999).
[8] T. Koga, J. Nitta, H. Takayanagi, and S. Datta, Phys. Rev. Lett. **88**, 126601 (2002).
[9] B. A. Gurney, in *Ultrathin Magnetic Structures IV*, edited by B. Heinrich and J. A. C. Bland (Springer, Berlin, 2005), p. 149.
[10] For an extensive review of electronic, optical, and transport properties of systems of reduced dimensions, such as quantum wells, wires, dots, and modulated 2D systems, see M. S. Kushwaha, Surf. Sci. Rep. **41**, 1 (2001).
[11] G. Lomer, F. Malcher, and U. Rossler, Phys. Rev. Lett. **60**, 728 (1988).
[12] J. Luo, H. Munekata, F. F. Fang, and P. J. Stiles, Phys. Rev. B **41**, 7685 (1990).
[13] D. Pines and P. Nozieres, *The Theory of Quantum Liquids* (Benjamin, New York, 1966); A. L. Fetter and J. D. Walecka, *Quantum Theory of Many-Particle Systems* (McGraw-Hill, New York, 1971); G. D. Mahan, *Many Particle Physics* (Plenum, New York, 1981).
[14] V. Fock, Z. Phys. **47**, 446 (1928); C. G. Darwin, Proc. Cambridge Philos. Soc. **27**, 86 (1930).
[15] F. Bloch, Z. Phys. **52**, 555 (1928).
[16] L. D. Landau, Z. Phys. **64**, 269 (1930).
[17] L. W. Shubnikov and W. J. de Haas, Leiden Commun. **207**, 210 (1930).
[18] W. J. de Haas and P. M. van Alphen, Leiden Commun. **212**, 215 (1930).
[19] R. B. Dingle, Proc. R. Soc. London, Ser. A **211**, 517 (1952); M. Ya. Azbel' and E. A. Kaner, Sov. Phys. JETP **3**, 772 (1956).
[20] D. Hofstadter, Phys. Rev. B **14**, 2239 (1976); D. Langbein, Phys. Rev. **180**, 633 (1969); P. G. Harper, Proc. R. Soc. London, Ser. A **68**, 879 (1955).
[21] K. von Klitzing, G. Dorda, and M. Pepper, Phys. Rev. Lett. **45**, 494 (1980); D. C. Tsui, H. L. Stormer, and A. C. Gossard, *ibid.* **48**, 1559 (1982).
[22] S. Murakami, N. Nagaosa, and S. C. Zhang, Science **301**, 1348 (2003).
[23] J. Sinova, D. Culcer, Q. Niu, N. A. Sinitsyn, T. Jungwirth, and A. H. MacDonald, Phys. Rev. Lett. **92**, 126603 (2004).
[24] J. Wunderlich, B. Kaestner, J. Sinova, and T. Jungwirth, Phys. Rev. Lett. **94**, 047204 (2005).
[25] W. K Tse and S. Das Sarma, Phys. Rev. Lett. **96**, 056601 (2006).
[26] K. W. Chiu and J. J. Quinn, Phys. Rev. B **9**, 4724 (1974).
[27] M. S. Kushwaha and S. E. Ulloa, Phys. Rev. B **73**, 205306 (2006).
[28] M. S. Kushwaha and S. E. Ulloa, Phys. Rev. B **73**, 045335 (2006).
[29] X. F. Wang, Phys. Rev. B **72**, 085317 (2005); G. Gumbs, *ibid.* **72**, 165351 (2005).
[30] C. A. Ullrich and M. E. Flatte, Phys. Rev. B **66**, 205305 (2002).
[31] I. S. Gradshteyn and I. M. Ryzhik, *Tables of Integrals, Series, and Products* (Academic, New York, 1994).
[32] S. Das Sarma, Phys. Rev. B **28**, 2240 (1984).